

# Cellulose Nanocrystal Inks for 3D Printing of Textured Cellular Architectures

Gilberto Siqueira, Dimitri Kokkinis, Rafael Libanori, Michael K. Hausmann, Amelia Sydney Gladman, Antonia Neels, Philippe Tingaut, Tanja Zimmermann,\* Jennifer A. Lewis,\* and André R. Studart\*

**3D printing of renewable building blocks like cellulose nanocrystals offers an attractive pathway for fabricating sustainable structures. Here, viscoelastic inks composed of anisotropic cellulose nanocrystals (CNC) that enable patterning of 3D objects by direct ink writing are designed and formulated. These concentrated inks are composed of CNC particles suspended in either water or a photopolymerizable monomer solution. The shear-induced alignment of these anisotropic building blocks during printing is quantified by atomic force microscopy, polarized light microscopy, and 2D wide-angle X-ray scattering measurements. Akin to the microreinforcing effect in plant cell walls, the alignment of CNC particles during direct writing yields textured composites with enhanced stiffness along the printing direction. The observations serve as an important step forward toward the development of sustainable materials for 3D printing of cellular architectures with tailored mechanical properties.**

## 1. Introduction

Direct ink writing (DIW) is an extrusion-based, 3D printing technique that enables programmable assembly of 3D architectures. Unlike conventional lithography, laser-based polymerization, or epitaxial assembly techniques, a broad range of materials can be printed at the microscale by this technique.<sup>[1,2]</sup> However, the development of viscoelastic inks that can be readily extruded, and yet form self-supporting features after

exiting the nozzle, is challenging. A viscoelastic response with a finite yield stress is required for filament patterning.<sup>[3]</sup>

The shear-induced alignment of anisotropic building blocks, including carbon fibers,<sup>[4,5]</sup> silicon carbide whiskers,<sup>[5]</sup> alumina platelets,<sup>[3]</sup> and nanofibrillated cellulose (NFC)<sup>[6]</sup> during direct ink writing enables the fabrication of textured 3D structured composites with enhanced mechanical properties and other functionalities. For cellulose-based materials, efforts to date have focused primarily on hydrogel-based inks that contain low NFC loading (0.8–2.5 wt%).<sup>[2,6–8]</sup> While the inherently entangled state of concentrated NFC suspensions prevent high loading, less concentrated NFC-filled inks typically

require thickening agents, such as fumed silica,<sup>[3]</sup> laponite,<sup>[6]</sup> or high molecular weight polymers,<sup>[9]</sup> to achieve the desired rheological properties for direct ink writing. By contrast, the use of cellulose nanocrystals (CNC) as a reinforcing agent in inks designed for 3D printing may offer advantages over the semicrystalline NFC, since higher solid loadings may be achieved at a given viscosity and storage modulus due to the absence of physical entanglements.<sup>[10]</sup>

Cellulose nanocrystals are discrete, anisotropic particles that possess a high aspect ratio (length-to-diameter ratio of 10–70) and outstanding mechanical properties. To date, they have been explored as reinforcing elements in synthetic composites.<sup>[11–13]</sup> CNC particles can be oriented in an applied electric field<sup>[14]</sup> or magnetic field,<sup>[15,16]</sup> as well as by mechanical shearing,<sup>[17]</sup> electrospinning,<sup>[18]</sup> or dry spinning.<sup>[19]</sup> However, these techniques are generally confined to producing 1D or 2D structures, such as fibers or films, respectively. Here, we create viscoelastic CNC-based inks for direct writing of textured cellular architectures. Both aqueous and monomer-based CNC inks (10–20 wt% solids) are developed, characterized, and printed into 3D structures. In both systems, shear-induced alignment of CNC particles is observed along the printing direction.

## 2. Results and Discussion

### 2.1. Structure and Rheological Properties of Aqueous-Based CNC Inks

CNC-based inks developed for direct writing must exhibit shear-thinning behavior to enable efficient flow through fine

Dr. G. Siqueira, M. K. Hausmann, Dr. A. Neels, Dr. P. Tingaut, Dr. T. Zimmermann  
Applied Wood Materials Laboratory and  
Center for X-ray Analytics  
Empa – Swiss Federal Laboratories for  
Materials Science and Technology  
Überlandstrasse 129  
CH-8600 Dübendorf, Switzerland  
E-mail: tanja.zimmermann@empa.ch  
D. Kokkinis, Dr. R. Libanori, Prof. A. R. Studart  
Complex Materials  
Department of Materials  
ETH Zürich  
8093 Zürich, Switzerland  
E-mail: andre.studart@mat.ethz.ch  
Dr. A. S. Gladman, Prof. J. A. Lewis  
School of Engineering and Applied Sciences and  
Wyss Institute for Biologically Inspired  
Engineering Harvard University  
Cambridge, MA 02138, USA  
E-mail: jalewis@seas.harvard.edu



DOI: 10.1002/adfm.201604619

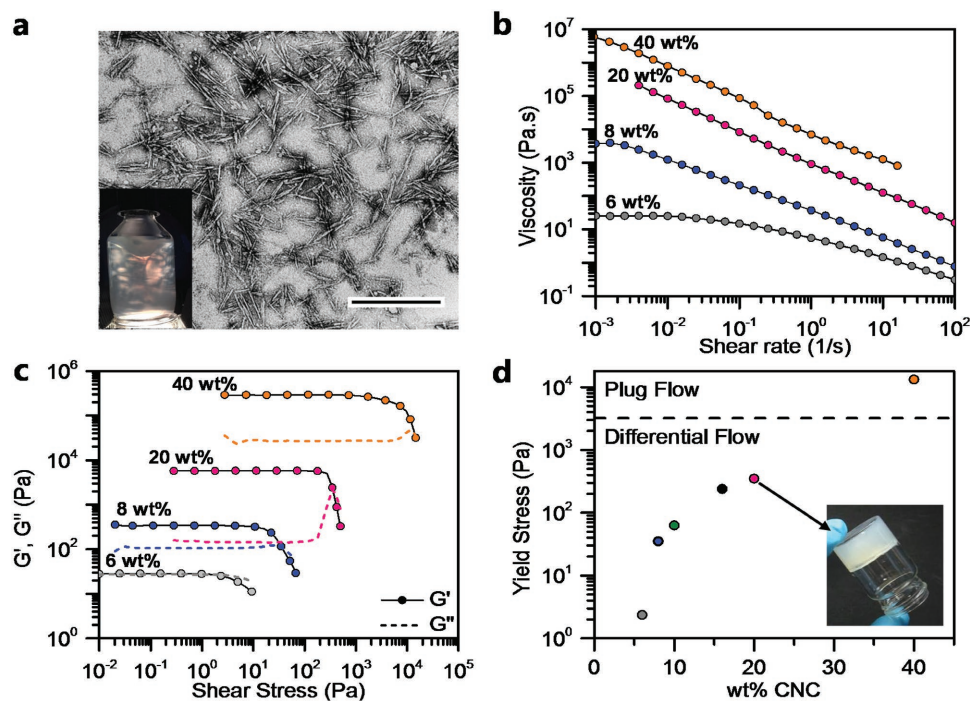


**Figure 1.** Morphology of wood pulp cellulose nanocrystals (CNC) and rheological behavior of aqueous CNC inks of varying solid loading. a) Transmission electron image of the anisotropic CNC particles (scale bar: 500 nm). Inset: photograph of an aqueous dispersion of wood pulp CNC (0.1 wt%) placed between cross-polarizers. b) Steady-shear and c) oscillatory rheological measurements (frequency = 1 Hz) for the aqueous CNC inks of increasing solid loading (6, 8, 20, and 40 wt% CNC). d) Shear yield stress of these CNC inks (Note: Dotted lines in (d) denote the transition from differential to plug flow. Inset: 20 wt% aqueous-based CNC ink in glass vial, 2.5 cm in diameter).

deposition nozzles, yet rapidly recovering a solid-like response with a sufficiently high storage modulus ( $G'$ ) and yield stress ( $\tau_y$ ) to maintain its filamentary shape upon printing.<sup>[5,20]</sup> To create aqueous inks, CNC are extracted from wood pulp and then dispersed in water using a planetary speed mixer (Figure 1a, inset). The CNC particles possess an aspect ratio,  $s$ , of about 18 with an average length ( $l$ ) and diameter ( $d$ ) of 120 and 6.5 nm, respectively. At high loadings (10–20 wt% CNC), these inks exhibit shear-thinning behavior without the need for other rheology modifiers. Figure 1b–d and Figure S1 (Supporting Information) show the rheological behavior of aqueous inks containing different concentrations of CNC. The onset of shear thinning behavior is observed at CNC concentration of 1 wt% (Figure S1, Supporting Information). However, inks composed of 8 wt% CNC or higher undergo pronounced shear thinning (Figure 1b and Figure S1 (Supporting Information)), in which their viscosity decreases by several orders of magnitude as the shear rate increases from 0.01 to 50  $s^{-1}$  (values typically applied during DIW).

Oscillatory measurements at low strains are carried out to assess the viscoelastic properties of aqueous CNC inks. These measurements reveal that dispersions with CNC concentrations higher than 6 wt% exhibit predominantly elastic behavior at low shear rates ( $G' > G''$ ) with a well-defined dynamic yield stress  $\tau_y$  (when  $G'' = G'$ ) (Figure 1c). Although all these dispersions could be used as inks for 3D printing, their high viscosity and shear yield stress can lead to prohibitively high printing pressures. When the maximum shear stress generated within the nozzle is not high enough to overcome the shear yield

stress, a plug flow regime develops, leading to an unyielded region of ink whose velocity remains constant. Under these conditions, CNCs would not be expected to align. Hence to optimize the degree of CNC alignment, we identified the optimal conditions for differential (shear) flow during direct ink writing.

To estimate the radial shear stress within the deposition nozzle ( $\tau$ ) during direct writing, we used the following equation<sup>[21]</sup>

$$\tau = \frac{\Delta P}{2L} r \quad (1)$$

where  $\Delta P$  is the maximum pressure applied at the nozzle,  $r$  is the radial position from the center to the edge of the nozzle, and  $L$  is the nozzle length. Substituting for the parameters of our 3D printer ( $\Delta P = 4 \times 10^5$  Pa;  $r = r_{\max} = 205 \times 10^{-6}$  m; and  $L = 1.27 \times 10^{-2}$  m), the calculated maximum shear stress ( $\tau_{\max}$ ) at the wall of the nozzle is 3228.3 Pa. Comparing the dynamic yield stresses of our CNC-based inks with the maximum shear stress developed in the nozzle (dotted line in Figure 1d), one finds that only inks that contain the highest CNC loading (40 wt%) experience plug flow (i.e.,  $\tau_y > \tau_{\max}$ ). For CNC loadings of 20 wt% or lower, one can use the yield stress data (Figure 1d) to estimate from Equation (1) the critical radius ( $r_c$ ) above which the ink is expected to undergo shear. Figure S2 (Supporting Information) shows that  $r_c$  increases from 2.23 to 22.2  $\mu\text{m}$  as the CNC concentration increases from 8 to 20 wt% for  $\Delta P = 4 \times 10^5$  Pa. Thus, we expect that 98.8 vol% of the ink



containing 20 wt% of CNC experiences shear forces during extrusion, which can lead to the desired filler alignment.

Hence, we used aqueous CNC inks (20 wt%) to print 3D cellular architectures. The 20 wt% CNC ink exhibits a plateau value of  $G' \approx 5.75 \times 10^3$  Pa that exceeds  $G''$  by about one order of magnitude at low shear stress (Figure 1c) and well-defined dynamic yield stress ( $\tau_y$ ) of 349 Pa, determined by the crossover point between the storage and loss moduli measured in oscillatory conditions at frequency of 1 Hz (Figure 1d).

## 2.2. Printing 3D Structures from Aqueous-Based CNC Inks

To illustrate direct writing of CNC-based inks, we printed 3D structures with different geometries using the formulation with 20 wt% CNC in water. The 3D printed structures contain between one and eight layers (Figure 2a,b and Figure S3 (Supporting Information)), each of which is composed of filamentary features (diameter = 410  $\mu\text{m}$ ) arrayed with a center-to-center spacing varying between 1.0 mm (grids) and 320  $\mu\text{m}$  (blocks). Upon drying, the resulting printed architectures consist of 100% CNC.

The shear-induced orientation of anisotropic CNC particles during printing is first investigated by optical microscopy in cross-polarized light mode (Figure 2c–e). Above a critical concentration, the CNC should undergo anisotropic crystalline ordering in aqueous suspensions in the absence of shear flow. Based on their aspect ratio of  $\approx 18$ , we expect anisotropic crystalline domains for CNC contents higher than 5 wt%.<sup>[11]</sup> As water slowly evaporates, the particles maintain their self-assembled liquid crystalline order during drying. This is experimentally confirmed by the birefringent regions (iridescence) observed in control samples composed of solution-cast films through cross-polarized light (Figure 1e).<sup>[11,22]</sup> This optical characteristic, first observed by Marchessault et al.,<sup>[22]</sup> provides a qualitative indication of strong CNC orientation within these films. Comparison of 3D printed structures to these films reveals that the shear-induced orientation of CNC particles along the printing direction further enhances their alignment, as reflected by the much smaller length scale of the birefringence effect and improved homogeneity of the ordered domains within the printed architectures.

To quantify the shear-induced CNC alignment, we carried out atomic force microscopy (AFM) and 2D wide-angle X-ray

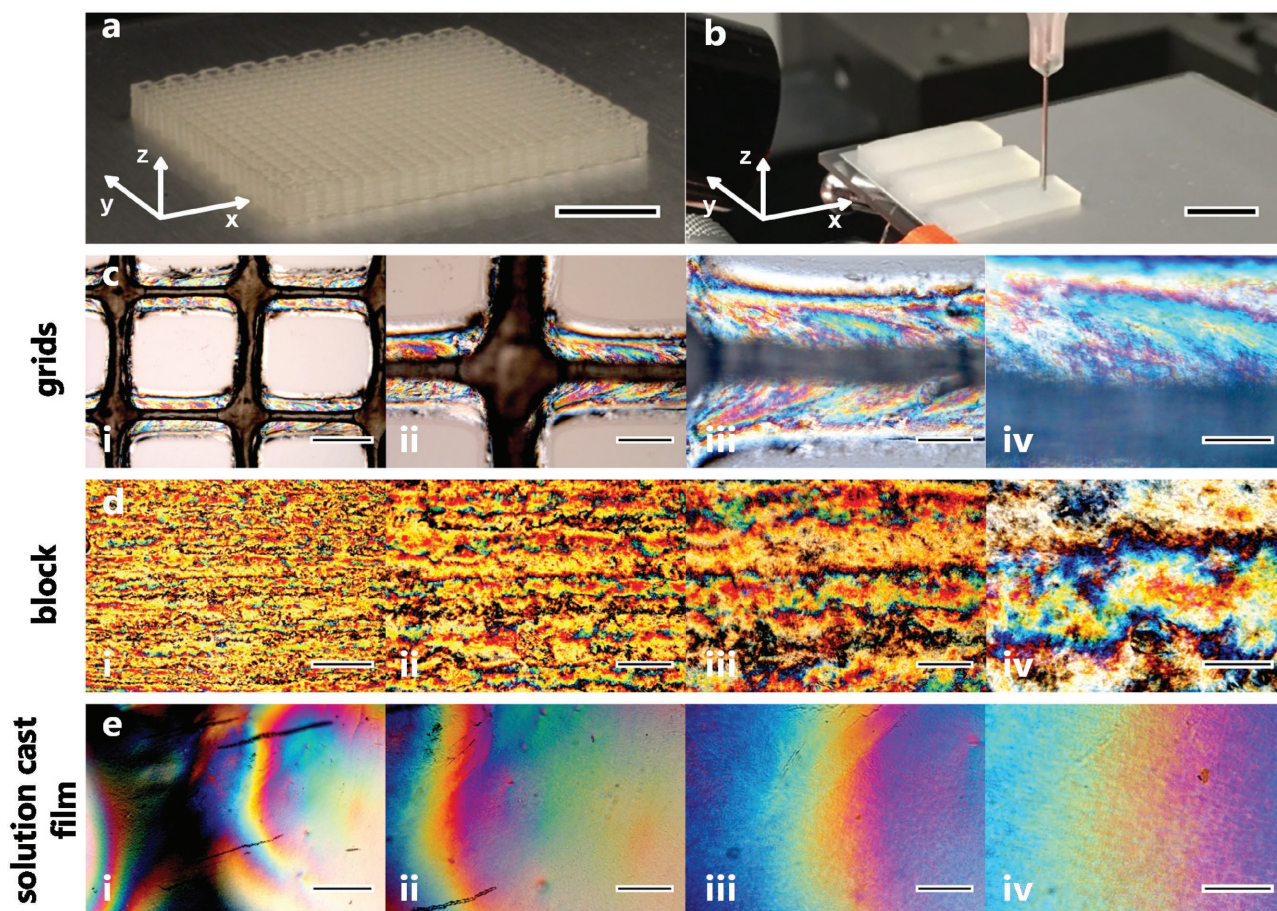


**Figure 2.** Printed CNC architectures after drying. a,b) Photographs of 3D printed (a) grids and (b) block composed of parallel lines in eight layers (scale bars: 10 mm). Optical microscopy images in cross-polarized light mode of CNC-based structures 3D printed into c) grids and d) top view of block. e) Films obtained by solution-casting are shown. Scale bars: i) 500  $\mu\text{m}$ , ii) 200  $\mu\text{m}$ , iii) 100  $\mu\text{m}$ , and iv) 50  $\mu\text{m}$ .

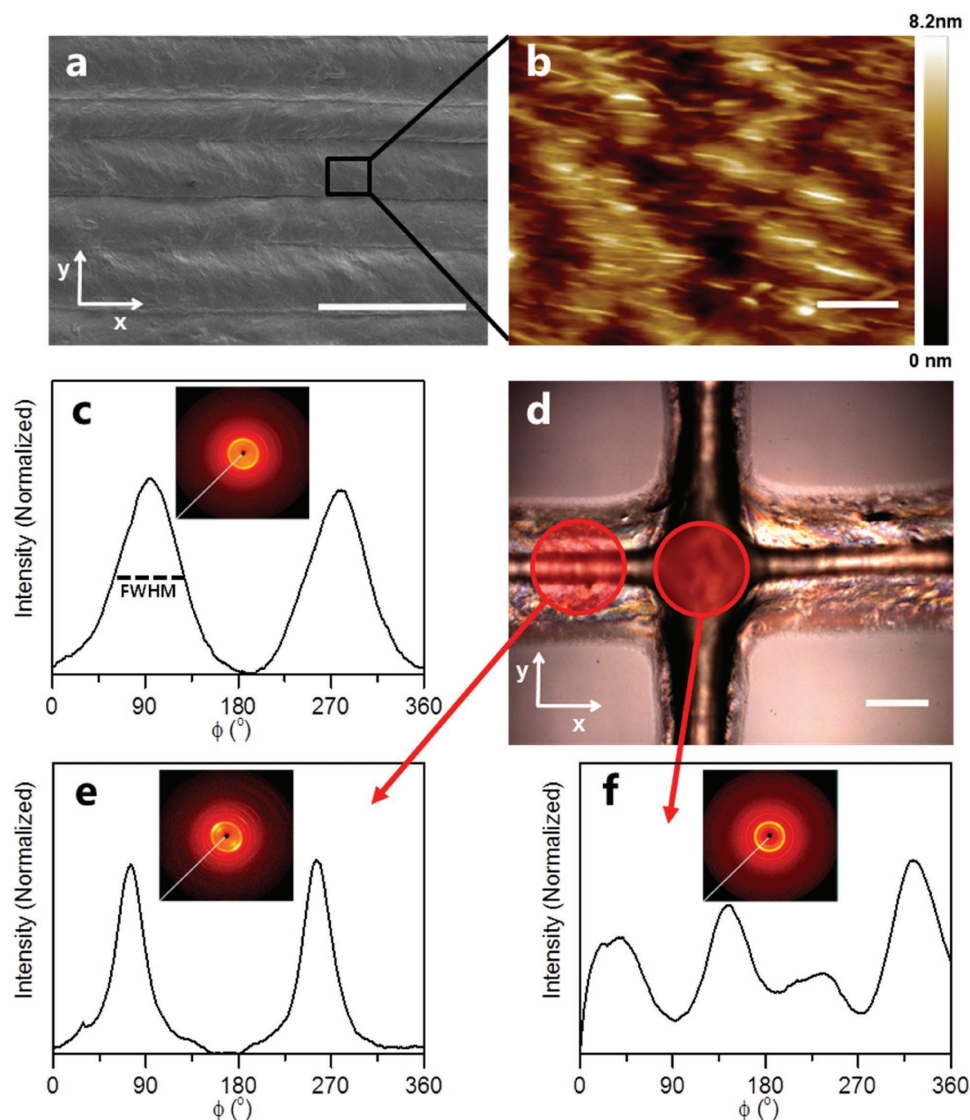


**Figure 3.** CNC alignment in 3D printed structures and control (solution-cast) films. a) SEM image showing printed filaments and their respective interfaces (scale bar: 200  $\mu\text{m}$ ). b) AFM topology (height image) of a single printed filament depicting preferential CNC alignment along the printing direction (scale bar: 100 nm). c,e,f) Normalized 2D-WAXS azimuthal intensity distributions of the equatorial reflection (200) of (c) a CNC film prepared by solution casting, (e) 3D printed CNC grids focused on the axial direction, and (f) 3D printed CNC grids focused on the cross-section of the filaments. The insets in (c), (e), and (f) show 2D-WAXS patterns. The grey line indicates sample orientation. d) Optical microscopy of 3D printed grid showing the beam spot where the scattering measurements (2D-WAXS) are performed along axial or cross-section directions. Scale bar: 200  $\mu\text{m}$ .

scattering (2D-WAXS) measurements of 3D printed filaments and as-cast films (Figure 3 and Figure S5 (Supporting Information)). We investigated different parameters, such as the degree of ordering ( $\pi$ ) and Herman's order parameter ( $f$ ), to determine the degree of CNC alignment in each structure.<sup>[23]</sup> These

calculated parameters are summarized in Table 1 (see Methods in the Experimental Section for details). In good agreement with the polarized light microscopy results, more pronounced CNC alignment is observed along the printing direction compared to solution-cast films, as indicated by lower full width

**Table 1.** CNC alignment in 3D printed architectures and cast films.

| Sample                               | FWHM [deg] | $1/\text{FWHM} \times 10^2$ [1/deg] | Degree of orientation, $\pi$ [%] | Herman's order parameter ( $f$ ) |
|--------------------------------------|------------|-------------------------------------|----------------------------------|----------------------------------|
| CNC solution cast film               | 68         | 1.47                                | 62                               | 0.34                             |
| CNC 3D printed blocks                | 46         | 2.17                                | 74                               | 0.56                             |
| CNC 3D printed grids axial direction | 28         | 3.57                                | 84                               | 0.65                             |
| CNC 3D printed grids cross-section   | 46         | 2.17                                | –                                | –                                |



**Table 2.** Nomenclature, CNC content, and tensile testing directions of the samples.

| Samples' name | Monomer | Oligomer   | Reinforcement [wt%] |              | Tensile test direction |
|---------------|---------|------------|---------------------|--------------|------------------------|
|               |         |            | Unmodified CNC      | Modified CNC |                        |
| M1            | HEMA    | PUA-BR751  | –                   | –            | Cast samples           |
| M1-10-L       | HEMA    | PUA-BR751  | 10                  | –            | Longitudinal           |
| M1-10-T       | HEMA    | PUA-BR751  | 10                  | –            | Transverse             |
| M1-10 Ac-L    | HEMA    | PUA-BR751  | –                   | 10           | Longitudinal           |
| M1-10 Ac-T    | HEMA    | PUA-BR751  | –                   | 10           | Transverse             |
| M1-20 Ac-L    | HEMA    | PUA-BR751  | –                   | 20           | Longitudinal           |
| M1-20 Ac-T    | HEMA    | PUA-BR751  | –                   | 20           | Transverse             |
| M2            | HEMA    | PUA-BR3741 | –                   | –            | Cast samples           |
| M2-10-L       | HEMA    | PUA-BR3741 | 10                  | –            | Transverse             |
| M2-10-T       | HEMA    | PUA-BR3741 | 10                  | –            | Longitudinal           |

at half maximum (FWHM) values, higher degree of ordering, and higher order parameters (Figure 3e,f and Table 1). Taken together, these data reveal that CNC particles spontaneously assemble into randomly distributed, long-range anisotropic domains within the plane of solution-cast films. Depending on the relative size of these domains to the beam size, preferential CNC orientation may be detected by 2D-WAXS (Figure 3c). By contrast, more pronounced CNC alignment along the longitudinal direction is observed within 3D printed samples, in which the resulting domains are preferentially oriented along a programmable printing direction.

### 2.3. Dispersion and Rheological Properties of Composite CNC Inks

To fabricate composite architectures with high CNC loading, we developed monomer-based inks composed of 10 or 20 wt% CNC dispersed in solution containing 2-hydroxyethyl methacrylate (HEMA) monomer, polyether urethane acrylate (PUA), and a photoinitiator that can be subsequently cured after printing by exposure to UV light. We selected monomers that exhibit good compatibility with unmodified CNC to obviate the need for solvent exchange.<sup>[24–26]</sup> In our approach, the initial water-based CNC suspension is diluted with an organic solvent and mixed directly with other ink constituents. Rotary evaporation is used to increase the concentration of CNC and reactive monomer constituents, as needed.

To further improve CNC dispersibility as well as the interfacial bonding between particles and matrix after polymerization, we also chemically modified the CNC surface using methacrylic anhydride (Figure S6, Supporting Information). This moiety undergoes an acetylation reaction with –OH groups on the cellulose surface and provides a vinyl functionality that can take part in the polymerization reaction of the monomer to covalent bond the particle and polymer matrix (Figures S7 and S8, Supporting Information). This modification also reduces hydrogen bonding between the CNCs, allowing the solid loading to be increased from 10 to 20 wt% in this ink. This leads to composites with higher transparency compared to those reinforced with unmodified CNC (Figure S9, Supporting Information).

However, the main disadvantage of chemically modified CNC inks is the need for solvent exchange from the reaction medium (*N,N*-dimethylformamide (DMF)) to ethanol/isopropanol to form a HEMA-CNC gel.

Two PUA oligomers are explored to obtain polymer matrices with either stiff, brittle (denoted by M1) to soft, rubbery (denoted by M2) responses, when tested uniaxially. For the sample nomenclature provided in Table 2, the M1 matrix consists of a 1:1 weight ratio of HEMA and PUA-BR751, whereas M2 matrix consists of a 1:1 weight ratio of HEMA and the PUA-BR3741, while the numbers 10 or 20 correspond to the CNC content (wt%) in each matrix. L is assigned to the samples tested in the longitudinal direction (printing direction) and T to samples tested in the transverse direction.

The rheological properties of our monomer-based CNC inks are shown in Figure 4a,b. These inks, which contain either 10 wt% of unmodified CNC or 10 to 20 wt% of acetylated CNC, exhibit viscosities that exceed  $10^4$  Pa s at low shear rates ( $0.01 \text{ s}^{-1}$ ) with strong shear thinning behavior (Figure 4a). Their high viscosities at low shear rates are reduced by three orders of magnitude when the ink is subjected to shear rates typically used in direct ink writing ( $\approx 50 \text{ s}^{-1}$ ).<sup>[5]</sup> The 10 wt% acetylated CNC ink has a lower viscosity ( $\approx 10^3$  Pa at  $0.01 \text{ s}^{-1}$ ) due to improved dispersion of acetylated CNC relative to the unmodified particles. The inks also exhibit viscoelastic behavior with plateau shear elastic modulus ( $G'$ ) ranging from  $3.3 \times 10^3$  to  $4.9 \times 10^4$  Pa and a well-defined dynamic shear yield stress ( $\tau_y$ ) ranging from 55 to 379 Pa (Figure 4b). Notably, using the same analysis described above, these CNC-polymer inks exhibit differential flow for the nozzle geometry and pressures using for DIW.

Good dispersion of CNCs within the polymer matrix (M1) was demonstrated by investigating fractured surfaces of pure polymer and 3D printed samples reinforced with 10 and 20 wt% of CNC (Figure 4c,d and Figure S10 (Supporting Information)). The small structures that are indicated by red arrows in Figure 4d are CNCs embedded in the polymer matrix. These small white dots have been previously reported in epoxy resin<sup>[13]</sup> as being the CNC's cross-sections distributed within the polymer matrix. Overall, the CNCs appear to be homogeneously distributed in the matrix of our composites.

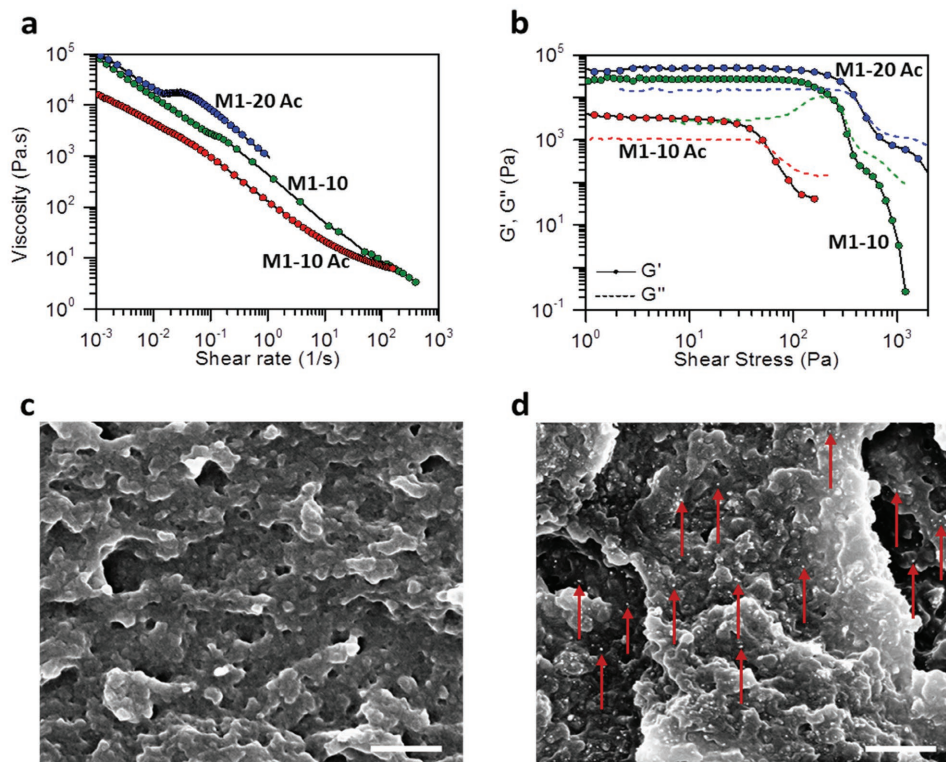


**Figure 4.** Development of monomer-based inks for printing composites with high volume fractions of CNC. Rheological data obtained under a) steady-shear and b) oscillatory conditions (1 Hz) for the monomer-based ink containing 10 and 20 wt% of CNC in a HEMA/PUA matrix 1 (M1). In the graphs of (a) and (b), the curves in green, red, and blue correspond to the inks prepared with matrix 1 (M1) reinforced with 10 wt% of unmodified CNC, 10 wt% of acetylated CNC, and 20 wt% of acetylated CNC, respectively. c,d) SEM images of fractured surfaces of matrix (M1) and 3D printed nanocomposites (20 wt% of acetylated CNC). Scale bars: 1  $\mu\text{m}$ . Red arrows indicate the cross-sections of CNC distributed in the matrix.

Although highly individualized CNCs are found throughout the fracture surface, the presence of small aggregates is also observed (Figure S10, Supporting Information).

#### 2.4. Printing 3D Structures from Composite CNC Inks

To determine the alignment of CNC particles within the polymer matrix, we carried out polarized light microscopy

(optical microscopy (OM)) and AFM measurements on the 3D printed filaments (Figure 5 and Figure S11 (Supporting Information)). These data confirm the alignment of the CNCs within the polymer-based composites. When the CNCs are aligned parallel to the polarized filter ( $0^\circ$ ), the linearly polarized light propagates through the sample without disturbance and is canceled out by the second polarized filter of opposite orientation (analyzer). As the sample is tilted from  $0^\circ$  to  $45^\circ$ , angle corresponding to the maximal transmittance, the lines become

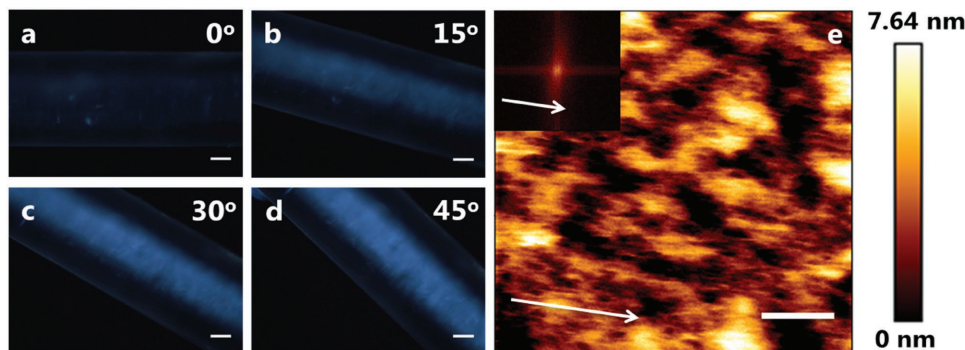


**Figure 5.** CNC alignment in printed composite filaments. a–d) Optical microscopy images in cross-polarized light mode (transmission) of CNC-based polymer filaments reinforced with 10 wt% CNC taken at (a)  $0^\circ$ , (b)  $15^\circ$ , (c)  $30^\circ$ , and (d)  $45^\circ$ . Scale bars in (a–d): 100  $\mu\text{m}$ . e) AFM height image of CNC-based composites indicating preferential orientation of CNC within the composites reinforced with 10 wt% CNC. Inset: Fourier transform of the AFM height image. Scale bar: 100 nm. White arrows indicate the preferential CNC orientation within the polymer matrix that corresponds to the printing direction [Note: The samples use matrix M1].

brighter due to enhanced light scattering by the aligned CNCs. We also investigated the degree of CNC alignment at the interface between two adjacent filaments that are printed to form a monolithic sample (Figure S12, Supporting Information). This interface appears brighter at 0°, indicating that the CNCs are slightly misaligned due to drag exerted by the passage of the nozzle during the deposition of the next line. Our analysis suggests that the interface between two filaments intermixes during direct writing promoting adhesion and thus does not require time-dependent diffusion of molecules to enable inter-filament bonding. Finally, the AFM images (Figure 5e and Figure S13 (Supporting Information)) and the accompanying Fourier transform reveal that CNC particles are oriented along the printing direction.

To experimentally investigate the effect of CNC alignment and reinforcement on mechanical properties, we printed CNC-filled composites with two different matrices: (M1) stiff, brittle matrix and (M2) soft, rubbery matrix. Figure 6a highlights typical stress–strain curves obtained for the pure matrices M1 and

M2 as well as 3D printed composite architectures. The reinforcing effect of CNC in polymer nanocomposites is evaluated using uniaxial tensile testing in the longitudinal (L) and transverse (T) orientations relative to the printing direction (Table 2). The elastic moduli ( $E$ ) of the materials are calculated from the slope of the initial elastic regime in each stress–strain curve. The results show that all M1-based composites exhibit a linear elastic regime, followed by a yield point and a strain hardening response before ultimate failure. By contrast, those based on the M2 matrix are similar to rubber-like materials, reaching larger elongations at break, but low tensile strengths.

While the pure matrix M1 is already quite stiff and strong, further reinforcement is possible using CNC particles (Figure 6). The most noticeable reinforcing effect is observed for strains beyond the yield point, where the CNC-based composites exhibit a more prominent strain hardening behavior compared to the pure matrix M1. By adding 10 wt% of unmodified or modified CNC to the polymer matrix (M1), the elastic modulus increases about 32% as compared to the neat

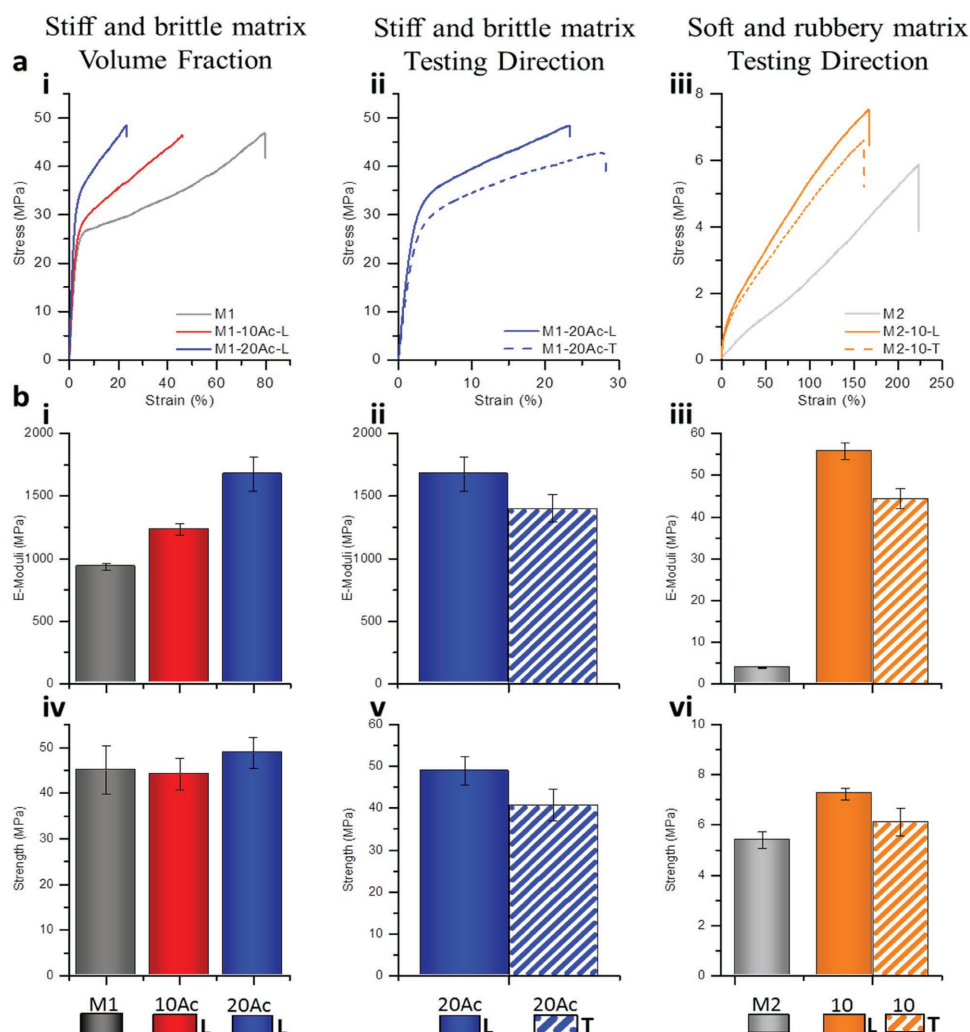


**Figure 6.** a) Representative stress–strain curves of the neat matrices and 3D printed nanocomposites prepared with matrices M1 and M2. b) Young's modulus ( $E$ ) (i–iii), and tensile strength ( $\sigma$ ) (iv–vi) of neat matrices M1 and M2 and 3D printed nanocomposites reinforced with 10 wt% of unmodified CNC, and 20 wt% of acetylated CNC tested in the longitudinal (L) and transverse (T) directions. Error bars show standard deviation ( $n = 9$ ).



matrix. Moreover, the elastic modulus increases by 80% when the matrix is reinforced with 20 wt% of modified CNC. Overall, the increase in elastic modulus is accompanied by a decrease in the strain at rupture, while the fracture strength remains nearly constant.

Interestingly, the mechanical tests also reveal a significant influence of the testing direction relative to the orientation of the filaments and of the embedded CNC (Figure 6). Such effects are observed in composites with 10 wt% CNC (Figure S14, Supporting Information) and become even more pronounced for those with 20 wt% CNC. During fabrication, each layer is printed and then UV cured (approximately a few minutes) to enhance the bonding between adjacent filaments. Hence, the enhanced mechanical properties in the longitudinal direction likely arise due to the orientation of the CNCs along the printed filament. Given their high aspect ratio (about 18) and degree of orientation, the CNCs are expected to enhance load transfer through shear stresses at the matrix-reinforcing elements interface leading to the observed anisotropic mechanical reinforcement.

To unambiguously assess the possible effect of interfilament bonding on the mechanical properties of composites tested in different orientations, we printed samples in the absence of CNC and probed their mechanical properties along distinct orientations relative to the printing direction (Figure S14, Supporting Information). The results indicate that the printing direction has no effect on their mechanical properties, confirming that the anisotropic response of the CNC-based composites arise from the orientation of the anisotropic particles inside the filaments. The relatively high mechanical properties of the composites tested in the transverse direction can be explained by the CNC misalignment at the interface between two printed filaments as indicated by the OM images of the composites (Figure 5). Such effect might be significantly reduced by optimizing the printing parameters to minimize the overlapping while still maintaining sufficiently strong connection of adjacent printing filaments. Our results also shed light into the role of CNC surface modification on the mechanical properties of the printed composites (Figure S15, Supporting Information). While the use of 10 wt% of surface modified CNCs is not increasing the elastic modulus relative to samples with unmodified CNC, the surface modification step allows one to create composites with higher CNC concentration of 20 wt%, which exhibit the best mechanical performance.

An even stronger reinforcing effect is expected using softer matrices such as natural rubber,<sup>[27]</sup> polystyrene-co-butyl acrylate,<sup>[12,28]</sup> or waterborne polyurethane.<sup>[29]</sup> To demonstrate this and the versatility of our method, we printed composites composed of a softer matrix (M2) reinforced with 10 wt% of unmodified CNC. Tensile testing of these nanocomposites confirms the more pronounced reinforcing effect of the CNC in a softer matrix (Figure 6). Compared to the pure matrix (M2), the elastic modulus increases by more than one order of magnitude, whereas their strength improves by 34% and 13% for specimens tested in the longitudinal and in the transverse directions, respectively. The mechanical properties of the printed materials can potentially be further improved by using CNC with higher aspect ratio or by increasing the CNC content in the inks, as demonstrated for the matrix 1 (M1).

### 3. Conclusions

We have demonstrated a route for 3D printing both pure CNC and CNC-reinforced composite architectures by direct writing of concentrated, viscoelastic aqueous and monomer-based CNC inks. This method yields cellulose-based structures with a high degree of CNC particle alignment along the printing direction. The capability can be exploited to create materials with programmable reinforcement along prescribed directions that exhibit tailored responses to the applied mechanical load, inspired by the design principles found in wood and other biological composites. This versatile approach opens new avenues for creating lightweight, sustainable composites with tailored architectures and mechanical properties.

### 4. Experimental Section

**Materials:** HEMA (98%), methacrylic anhydride (94%), and pyridine were purchased from Sigma-Aldrich. The difunctional PUA oligomers PUA-BR571 and PUA-BR3741A], and the photoinitiator bis(2,4,6-trimethylbenzoyl)-phenylphosphineoxide (Irgacure 819) were supplied by Dymax and BASF, respectively. DMF ( $\geq 99.5\%$  synthesis) was purchased from Roth AG. Hydrophobic pyrogenic silica HDK H18 was obtained from Wacker Chemie AG. CNCs were prepared via sulfuric acid hydrolysis of eucalyptus pulp at the USDA Forest Service – Forest Products Laboratory (Madison, WI), according to the procedures described by Beck-Candanedo et al.<sup>[30]</sup>

**Chemical Modification of CNC:** Freeze-dried CNCs were dispersed in DMF in order to form a 21 wt% gel. The mixture was placed in the speed mixer (SpeedMixer DAC 150.1 FVZ) for 5 min at 2000 and 3500 rpm, left overnight, and speed-mixed again. 141 g of DMF was added to 15.7 g of CNC/DMF gel and dispersed with a magnetic stirrer in a glass reactor with condensation reflux until a homogeneous solution (2 wt% CNC) was obtained. This solution was heated to 105 °C under continuous nitrogen flow. Once the desired temperature was reached, 188.9 g of methacrylic anhydride and 4.8 g of pyridine were added and the reaction was left for 5 h. At the end of the reaction, the modified material was washed four times with a mixture of toluene/acetone/ethanol (4:1:1) using a centrifuge at 5000 rpm and 5 °C for 25 min. The precipitated modified CNCs were subsequently solvent exchanged with isopropanol for further use. Solvent exchange was accomplished following three centrifuge cycles.

#### Methods:

**CNC-Based Inks: Aqueous-Based CNC Inks:** Different concentrations of CNC suspensions/gels, from 0.5 to 40 wt% were prepared with specific amounts of freeze-dried CNC and deionized water. The materials were homogenized using a planetary centrifugal speed mixer at 800, 1500, and 2250 rpm for 2 min. The homogenization step was repeated two times.

**Inks for Nanocomposite Fabrication (CNC-Based Inks Designed with Matrix 1):** The ink formulation used for the preparation of polymer-based composites contained the following main components: HEMA monomer, PUA oligomer (BR751), photoinitiator, and CNC. CNCs were dispersed in a water/HEMA mixture. To enable the preparation of CNC-based nanocomposites, 25 g of the initial 20 wt% water based CNC-ink was diluted with 75 g of deionized water. 20 g of HEMA monomer was added to the mixture. The mixture was stirred for 5 min and sonicated for 2 min. The water was evaporated by using a rotavapor at 60 °C under pressure of 30 mbar, leading to a 20 wt% HEMA/CNC gel. Thereafter, 6.7 g of the oligomer (PUA) was mixed with 8.2 g of the HEMA /CNC gel. The resulting HEMA/PUA-CNC gel was further mixed with 0.5 wt% of the photoinitiator (Irgacure 819) in a planetary mixer (ARE-250, Thinky) at 2500 rpm for 1 h with two ceramic spheres in the container and processed three times on a three roll-mill (DSY-200, Bühler, Switzerland). The resulting material was again homogenized



in the planetary mixer at 2500 rpm for 5 min. The final ink contained 10 wt% of CNC. The inks containing 10 or 20 wt% of functionalized CNC were prepared following the same protocol with the exception that the HEMA/CNC gel was prepared in a mixture of isopropanol/ethanol (3:1) instead of water.

Matrix 1 filled with isotropic fumed silica was prepared by mixing 9.155 g of HEMA, 9.155 g of PUA-BR751, 0.09 g of photoinitiator, and 1.6 g of fumed silica.

As a reference, the matrix 1 (M1) alone was prepared by mixing 8.955 g of HEMA, 8.955 g of PUA-BR751, and 0.09 g of photoinitiator.

**Inks for Nanocomposite Fabrication (CNC-Based Ink Designed with Matrix 2):** The ink formulated using matrix 2 contained 10 wt% of unmodified CNC and its preparation followed the same procedure developed for matrix 1, except that the oligomer used was the PUA-BR3741A).

As a reference, the matrix 2 (M2) alone was prepared by mixing 8.955 g of HEMA, 8.955 g of PUA-BR3741A), and 0.09 g of photoinitiator.

#### 3D Printing:

Prior to printing tests, the inks were loaded into 5 mL syringes and centrifuged at 3600–4500 rpm for 3 min to remove bubbles.

**All Cellulose-Based Materials:** Loaded syringes containing the 20 wt% water-based CNC ink were mounted in a 3D printer (ABL 900010, Aerotech Inc., Pittsburgh, PA) and the ink was driven pneumatically through micronozzles of different sizes (200–410  $\mu\text{m}$ ). The inks were printed onto a hydrophobized glass slide, and extruded under pressures ranging from 2 to 4 bar at a speed of 10–20  $\text{mm s}^{-1}$ .

**CNC-Nanocomposites:** Syringes loaded with CNC polymer-based ink were mounted in the 3D printer (3D Discovery, RegenHU Ltd., Switzerland). Ink was driven pneumatically and extruded through a micronozzle (410  $\mu\text{m}$ ) onto hydrophobized glass substrates under an applied pressure of 3–4 bar, at a speed of 10  $\text{mm s}^{-1}$ . After printing, the materials were cured with UV light under nitrogen ( $\text{N}_2$ ) atmosphere to avoid oxygen inhibition of the polymerization reaction.

#### Microstructural Characterization:

**Transmission Electron Microscopy (TEM):** The morphology of the CNCs used as source for the 3D printing inks was characterized by TEM (Jeol JEM-2200FS, USA Inc.) using an acceleration voltage of 200 kV. A drop of diluted suspension of the cellulose nanocrystals was deposited onto a carbon-coated grid. The samples were stained with a 2 wt% solution of uranyl acetate. The average diameter and length of the CNC were measured using the measuring tool in Image J software.

**Optical Microscopy:** Confocal OM (Zeiss LSM710) was used to observe the diameter and the surface morphology of printed architectures and the appearance of the 3D printed filaments. Flow birefringence of CNC within the 3D printed filaments was observed in digital microscopes (Leica DVM 2500 and Zeiss LSM710) equipped with cross-polarizers. The CNC orientation within the polymer composites was qualitatively evaluated by OM through cross-polarized light in transmission mode (Zeiss LSM710).

**Atomic Force Microscopy:** AFM height and phase images were used to access the CNC ordering in the 3D printed filaments (blocks) in the all cellulose-based materials. The all cellulose-based structures were investigated with a Multimode Nanoscope VIII, in tapping mode, using tips PPP-NCLR-20, Nanosensors, a spring constant of 21–98  $\text{N m}^{-1}$ , and a resonance frequency of 146–236 kHz. The polymer-based CNC composites were analyzed with a Multimode Nanoscope 8, in quantitative mode (setpoint 50 nN, z length 100 nm, pixel time 8 ms, tip radius 10 nm).

**Scanning Electron Microscopy:** Scanning electron microscopy (SEM) was performed on samples of 0.5 cm in length glued with carbon adhesive tape onto aluminum sample holders. A thin platinum layer ( $\approx 2$  nm) was deposited on the materials' surface. A FEI Nova NanoSEM 230 instrument (FEI, Hillsboro, OR) was used at an accelerating voltage of 5 kV and a working distance of 5 mm. The analyses were performed to determine the surface morphology of the water-based printed structures. The fractured surfaces of the nanocomposites were also analyzed by SEM in order to verify the CNC distribution in the polymer matrix.

**Fourier Transform Infrared Spectroscopy:** Infrared spectra of dried unmodified and acetylated CNC (i.e., dried at 105  $^{\circ}\text{C}$  for 12 h) were recorded in a FTS 6000 spectrometer (Portmann Instruments AG) in attenuated total reflectance mode. The spectra were recorded between 4000 and 500  $\text{cm}^{-1}$ , with a resolution of 4  $\text{cm}^{-1}$  and 32 scans.

**$^{13}\text{C}$  CP-MAS NMR Spectroscopy:** Solid state Cross-Polarization Magic Angle Carbon-13 Nuclear Magnetic Resonance ( $^{13}\text{C}$  CP-MAS NMR) spectrum of acetylated CNC was recorded at room temperature on a Bruker Avance 400 NMR spectrometer (Bruker Biospin AG), using a MAS rate of 3 kHz. The spectra were run for 12 h (15 000 scans).

#### Physical Characterization:

**Rheology of Aqueous-Based Inks:** The rheological properties of the inks were determined using an AR 2000ex rheometer (TA Instruments, New Castle, USA) with a 60 mm cone plate geometry for suspensions with solid content ranging from 0.5 to 20 wt% and 20 mm parallel plate geometry for the samples with solid content of 40 wt%. Dynamic measurements were performed in the frequency range of 0.1–100 Hz and at a temperature of 25  $^{\circ}\text{C}$ . The elastic shear ( $G'$ ) and viscous ( $G''$ ) moduli were measured using an oscillatory logarithmical stress sweep at the frequency of 1 Hz. An aqueous solvent trap was utilized in all experiments to mitigate drying effects.

**2D-WAXS:** 2D wide-angle X-ray scattering had been carried out with a STOE IPDS-II instrument using Mo  $K\alpha$  radiation ( $\lambda = 0.71073$   $\text{\AA}$ , 40 mA, 50 kV, beam diameter of 0.5 and 0.3 mm). The degree of CNC alignment within the printed filaments was studied. The printed filaments were fixed on the goniometer head and then placed perpendicular to the beam to allow the X-rays to pass through the filaments only. The samples were exposed for 5 min in transmission mode and the 2D-WAXS data were collected using an image plate system with a sample to detector distance of 200 mm resulting in a  $2\theta$  range from  $2^{\circ}$  to  $40^{\circ}$ . The patterns were corrected for air scattering and backgrounded by subtracting a no-sample diffraction pattern from the raw data.

Two types of orientation factors, the degree of orientation ( $\pi$ ), and the Herman's order parameter ( $f$ ) were calculated from the azimuthal intensity distribution profiles according to Equations (2), (3), (4), (5).<sup>[23]</sup> FWHM is the full width at half maximum. The distribution of intensity ( $I$ ) with respect to ( $\phi$ ) along the  $360^{\circ}$  circle, defined by  $2\theta = 21.0^{\circ}$ – $22.3^{\circ}$ , refers to the (200) reflection of the cellulose I $\beta$  crystals. In addition, the Herman's order parameter ( $f$ ) was calculated assuming asymmetric orientation. An order parameter of  $f = 1$  corresponds to a maximum orientation of CNC along the printed filaments, while  $f = 0$  indicates random orientation of CNC

$$\pi = \frac{180 - \text{FWHM}}{180} \quad (2)$$

$$f = \frac{3\langle \cos^2 \gamma \rangle - 1}{2} \quad (3)$$

where

$$\langle \cos^2 \gamma \rangle = 1 - 2\langle \cos^2 \theta \rangle \quad (4)$$

and

$$\langle \cos^2 \theta \rangle = \frac{\int I(\phi) \cos^2 \phi \sin \phi \, d\phi}{\int I(\phi) \sin \phi \, d\phi} \quad (5)$$

**Mechanical Properties of Nanocomposites:** Standard dog bone samples were punched out of 300–350  $\mu\text{m}$  thick films with the tested region being 12 mm  $\times$  2 mm. Tensile tests were carried out in a universal mechanical testing machine (Shimadzu AGS-X, Japan), equipped with a 100 N load cell. The samples were dried in oven overnight at temperature of 60  $^{\circ}\text{C}$ . The tests were conducted using a constant speed of 5  $\text{mm min}^{-1}$  at relative humidity of  $\approx 58\%$  and temperature of  $\approx 25$   $^{\circ}\text{C}$ . A minimum of nine samples out of three films was used to characterize each material.

## Supporting Information

Supporting Information is available from the Wiley Online Library or from the author.

## Acknowledgements

The authors thank Esther Strub for her support with SEM imaging of printed blocks, Anja Huch for the help with TEM of CNC solutions, Dr. Solenne Deseaux and Kirstin Casdorff for AFM imaging, and Daniel Rentsch for the NMR measurements. The authors also acknowledge the financial support from the Swiss National Science Foundation (grant 200021-159906/1), the Air Force Office of Scientific Research (grant FA9550-16-1-0007), and the Swiss Competence Center for Energy Research (SCCER – Capacity Area A3: Minimization of energy demand). A.S.G. and J.A.L. were supported by the Army Research Office Award No. W911NF-13-0489.

Received: September 6, 2016

Revised: November 28, 2016

Published online:

- [1] G. M. Gratson, J. A. Lewis, *Langmuir* **2005**, *21*, 457.
- [2] K. Markstedt, A. Mantas, I. Tournier, H. M. Avila, D. Hagg, P. Gatenholm, *Biomacromolecules* **2015**, *16*, 1489.
- [3] D. Kokkinis, M. Schaffner, A. R. Studart, *Nat. Commun.* **2015**, *6*, 1.
- [4] H. L. Tekinalp, V. Kunc, G. M. Velez-Garcia, C. E. Duty, L. J. Love, A. K. Naskar, C. A. Blue, S. Ozcan, *Compos. Sci. Technol.* **2014**, *105*, 144.
- [5] B. G. Compton, J. A. Lewis, *Adv. Mater.* **2014**, *26*, 5930.
- [6] A. S. Gladman, E. A. Matsumoto, R. G. Nuzzo, L. Mahadevan, J. A. Lewis, *Nat. Mater.* **2016**, *15*, 413.
- [7] B. C. Wang, A. J. Benitez, F. Lossada, R. Merindol, A. Walther, *Angew. Chem. Int. Ed.* **2016**, *55*, 5966.
- [8] J. G. Torres-Rendon, T. Femmer, L. De Laporte, T. Tigges, K. Rahimi, F. Gremse, S. Zafarnia, W. Lederle, S. Ifuku, M. Wessling, J. G. Hardy, A. Walther, *Adv. Mater.* **2015**, *27*, 2989.
- [9] J. T. Muth, D. M. Vogt, R. L. Truby, Y. Menguc, D. B. Kolesky, R. J. Wood, J. A. Lewis, *Adv. Mater.* **2014**, *26*, 6307.
- [10] K. J. Le Goff, D. Jouanneau, C. Garnier, T. Aubry, *J. Appl. Polym. Sci.* **2014**, *131*, 40676.
- [11] A. Dufresne, *Nanocellulose: From Nature to High Performance Tailored Materials*, Walter de Gruyter GmbH, Berlin **2012**.
- [12] V. Favier, H. Chanzy, J. Y. Cavaille, *Macromolecules* **1995**, *28*, 6365.
- [13] L. M. Tang, C. Weder, *ACS Appl. Mater. Interfaces* **2010**, *2*, 3396.
- [14] D. Bordel, J.-L. Putaux, L. Heux, *Langmuir* **2006**, *22*, 4899.
- [15] J. Sugiyama, H. Chanzy, G. Maret, *Macromolecules* **1992**, *25*, 4232.
- [16] T. Pullawan, A. N. Wilkinson, S. J. Eichhorn, *Biomacromolecules* **2012**, *13*, 2528.
- [17] J. A. Diaz, X. Wu, A. Martini, J. P. Youngblood, R. J. Moon, *Biomacromolecules* **2013**, *14*, 2900.
- [18] N. V. Herrera, A. P. Mathew, L. Y. Wang, K. Oksman, *Plast., Rubber Compos.* **2011**, *40*, 57.
- [19] S. Chen, G. Schueneman, R. B. Pipes, J. Youngblood, R. J. Moon, *Biomacromolecules* **2014**, *15*, 3827.
- [20] A. R. Studart, *Chem. Soc. Rev.* **2016**, *45*, 359.
- [21] J. S. Reed, *Introduction to the Principles of Ceramic Processing*, John Wiley and Sons Ltd, New York, United States, **1988**.
- [22] R. H. Marchessault, F. F. Morehead, N. M. Walter, *Nature* **1959**, *184*, 632.
- [23] N. Yoshiharu, K. Shigenori, W. Masahisa, O. Takeshi, *Macromolecules* **1997**, *30*, 6395.
- [24] Y. Habibi, A.-L. Goffin, N. Schiltz, E. Duquesne, P. Dubois, A. Dufresne, *J. Mater. Chem.* **2008**, *18*, 5002.
- [25] G. Morandi, L. Heath, W. Thielemans, *Langmuir* **2009**, *25*, 8280.
- [26] O. van den Berg, J. R. Capadona, C. Weder, *Biomacromolecules* **2007**, *8*, 1353.
- [27] A. Bendahou, Y. Habibi, H. Kaddami, A. Dufresne, *J. Biobased Mater. Bioenergy* **2009**, *3*, 81.
- [28] V. Favier, J. Y. Cavaille, H. Chanzy, A. Dufresne, *Abstr. Pap. Am. Chem. Soc.* **1995**, *209*, 29.
- [29] X. Cao, H. Dong, C. M. Li, *Biomacromolecules* **2007**, *8*, 899.
- [30] S. Beck-Candanedo, M. Roman, D. G. Gray, *Biomacromolecules* **2005**, *6*, 1048.